

23

Modeling of Resonators

§23.1 A GENERIC RESONATOR

A second example where simplified discrete modeling has been found valuable is in the assessment of the performance of micro-electro-mechanical system (MEMS) resonators. Of several available resonator models, we will consider a double-beam resonator. When the input beam which acts as a conductor is placed under alternating voltage field, the input beam vibrates with the exciting voltage frequency, possibly with all the frequency ranges of the input frequency. The motion of the input beam then triggers motion of the output beam through the link element as shown in Fig. 23.1. In doing so, the link acts as a filter and triggers the output beam to resonate with its fundamental frequency, thus extracting an almost single-tone frequency. Consequently, the double beam resonator has an inherent "frequency filtering" capability.

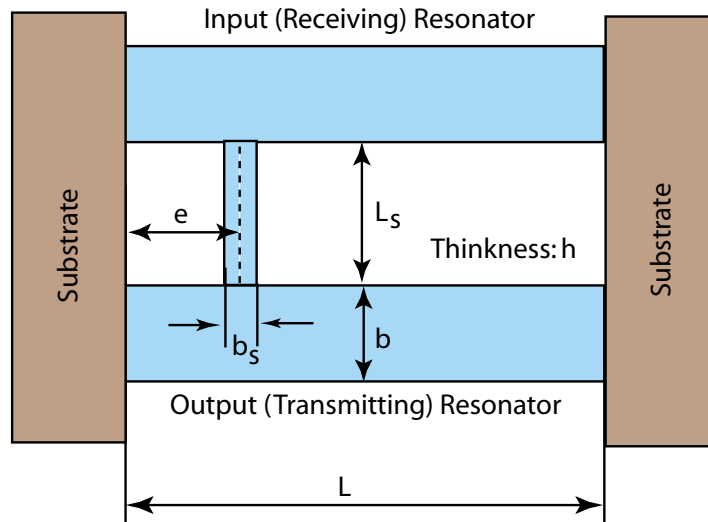


Figure 23.1: A Double Beam Resonator

§23.2 ONE-DOF MODELING OF A SINGLE BEAM

Consider one of the resonator with fixed-fixed ends. As we are interested in modeling the beam with one degree of freedom, we sample the displacement at the beam center and represent the motion of the beam center with an equivalent mass and stiffness. There are two ways of reducing the beam dynamics: order reduction via the finite element method and mass and stiffness lumping from the continuum beam equation. In this section we will employ the continuum beam solution and adapt it to the present task. To this end, we recall that the transverse beam displacement, $w(x, t)$, is expressed as

$$w(x, t) = C_1(t) \sin \beta x + C_2(t) \cos \beta x + C_3(t) \sinh \beta x + C_4(t) \cosh \beta x \quad (23.1)$$

$$(\beta L) = 4.71$$

The three unknown coefficients (C_2, C_3, C_4) can be expressed in terms of C_1 by applying the boundary conditions

$$w(0, t) = \frac{\partial w(0, t)}{\partial x} = w(L, t) = \frac{\partial w(L, t)}{\partial x} = 0 \quad (23.2)$$

When this is carried out, the transverse displacement reads:

$$w(x, t) = \Phi(x) C_1(t)$$

$$\Phi(x) = (\sin \beta x - \sinh \beta x) + \frac{(\sin \beta L - \sinh \beta L)}{(\cos \beta L - \cosh \beta L)} (\cos \beta x - \cosh \beta x) \quad (23.3)$$

Observe that $C_1(t)$ can be related to the mid-span displacement, $w(L/2, t)$ from the above equation:

$$w(t) = w(L/2, t) = \Phi(L/2)C_1(t)$$

$$\Downarrow$$

$$w(x, t) = N(\beta L, x) w(t), \quad N(\beta L, x) = \frac{\Phi(x)}{\Phi(L/2)} \quad (23.4)$$

The above equation can now be used to obtain equivalent stiffness and mass properties for a single degree of freedom model as follows.

Observe that the kinetic and potential energy can be obtained by

$$T = \frac{1}{2}m \dot{w}^2 = \frac{1}{2}\dot{w} \left[\int_0^L \rho A N^2(\beta L, x) dx \right] \dot{w}$$

$$V = \frac{1}{2}k w^2 = \frac{1}{2}w \left[EI \int_0^L N_{xx}^2(\beta L, x) dx \right] w \quad (23.5)$$

Upon evaluating the integrals in the above equation, we find that

$$k_b = \frac{192EI}{L^3}, \quad m_b \approx 0.3836 (\rho AL) \quad (23.6)$$

It should be noted that the preceding (m_b, k_b) closely satisfies the classical frequency equation. To see this we first compute the natural frequency of the single degree of freedom model:

$$\omega_n^2 = k_b/m_b = \left(\frac{192}{0.3836} \right) \frac{EI}{\rho AL^4} \quad (23.7)$$

Observing the classical frequency equation

$$(\beta L)^4 = (4.73)^4 = \omega^2 \frac{\rho A}{EI} L^4 \quad (23.8)$$

it is clear the constant $\left(\frac{192}{0.3836} \right)$ in the one degree-of-freedom case should be as close as possible to the continuum case $(\beta L)^4$.

$$\left(\frac{192}{0.3836} \right) = 500.5214 \quad vs. \quad (\beta L)^4 = 500.5467 \quad (23.9)$$

yielding 0.005 % error, which is quite adequate.

It should be emphasized that the mass and stiffness properties obtained in (23.6) are applicable to both resonating beam as they are for most cases identical. The remainder is to model the linking beam and a procedure to couple the linking beam to the two resonating beams.

§23.3 MODELING OF THE LINKING BEAM

For this case we first treat the beam ends with the following boundary conditions:

$$\frac{\partial^3 w(0, t)}{\partial x^3} = \frac{\partial w(0, t)}{\partial x} = \frac{\partial^3 w(L, t)}{\partial x^3} = \frac{\partial w(L, t)}{\partial x} = 0 \quad (23.10)$$

which allow a free transverse movement at both ends while the rotations are constrained as shown in Fig. 23.2. The fundamental frequency for this case can be obtained by the continuum beam frequency solution method described in Lecture 13 by setting the end springs as

$$k_{w1} = k_{w2} = 0, \quad k_{\theta1} = k_{\theta2} = \infty \quad (23.11)$$

which yields

$$\beta L = \pi \quad (23.12)$$

for its fundamental frequency.

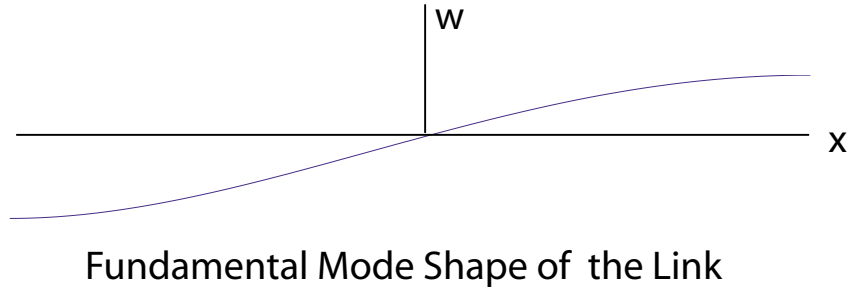


Figure 23.2: Fundamental Mode Shape of the Link Element

It should be noted that the other mode is a translational rigid-body mode. In other words, when the link beam undergoes a rigid-body mode, the two resonating beams move in phase.

On the other hand, when the link beam deforms in its fundamental frequency mode, the two resonating beams will move out of phase. Of course for this case, the link beam will experience twisting, which is not considered in the present model. We will revisit this phenomenon later in the analysis of the complete coupled system.

One important difference between the linking beam model and the resonator is that the linking beam must be modeled in terms of its two-end displacements without any rotational motion degrees of freedom. This can be done as

$$\begin{aligned} k_{link} &= k_s \begin{bmatrix} 1 & -1 \\ -1 & 1 \end{bmatrix}, \quad k_s = \frac{12EI_s}{L_s^3} \\ m_{link} &= \alpha m_s \begin{bmatrix} 1 & 0 \\ 0 & 1 \end{bmatrix}, \quad m_s = \rho A_s L_s, \quad \alpha = 0.2464 \end{aligned} \quad (23.13)$$

where α is a correction factor to fit the fundamental frequency of the linking beam, viz., $\beta L_s = \pi$.

§23.4 COUPLING OF THE LINK BEAM TO THE TWO RESONATING BEAMS

We have completed the individual modeling of the two resonator beams and the linking beam. For illustrative purposes the in-phase and out-of-phase motions of the system are shown in Figs. 23.3 and 23.4. Observe that for the case of in-phase mode the linking beam acts as a rigid link, whereas of out-of-phase mode the linking beam undergoes its fundamental mode shape.

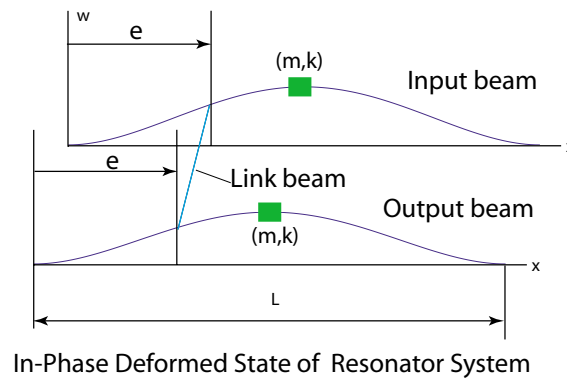


Figure 23.3: In-Phase Deformed State of Double Beam Resonator

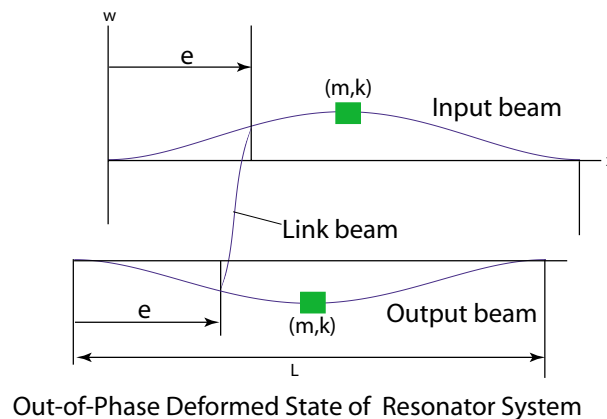


Figure 23.4: Out-of-Phase Deformed State of Double Beam Resonator

An equivalent mass-spring model that accounts for both motions may be represented as shown in Fig. 23.5.

The starting point for the development of an equivalent mass-damper-spring model from the skeletal model is to obtain the kinetic and potential energies of the two systems:

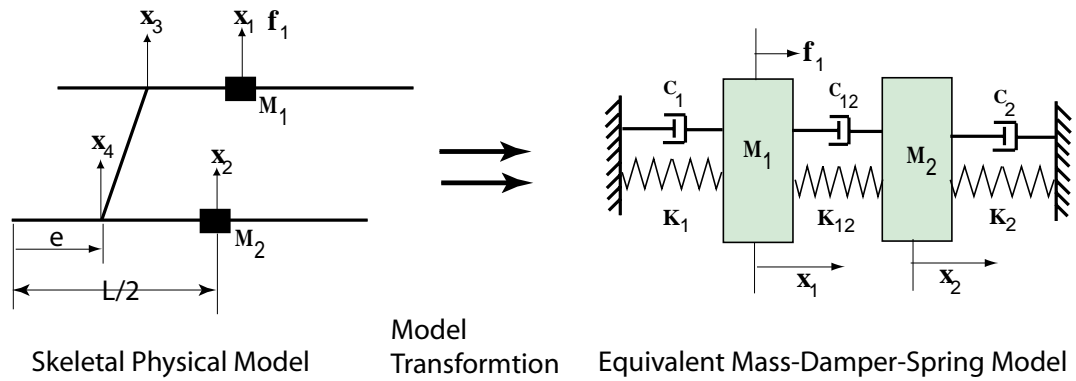


Figure 23.5: Physical and Equivalent Mass-Damper-Spring Model

Skeletal Model:

$$T_s = \frac{1}{2}m_b\dot{x}_1^2 + \frac{1}{2}m_b\dot{x}_2^2 + \frac{1}{2} \begin{bmatrix} \dot{x}_3 \\ \dot{x}_4 \end{bmatrix}^T [m_{link}] \begin{bmatrix} \dot{x}_3 \\ \dot{x}_4 \end{bmatrix} \quad (23.14)$$

$$K_s = \frac{1}{2}k_b x_1^2 + \frac{1}{2}k_b x_2^2 + \frac{1}{2} \begin{bmatrix} x_3 \\ x_4 \end{bmatrix}^T [k_{link}] \begin{bmatrix} x_3 \\ x_4 \end{bmatrix}$$

Mass-Damper-Spring Model:

$$T_{mdk} = \frac{1}{2}M_1\dot{x}_1^2 + \frac{1}{2}M_2\dot{x}_2^2 \quad (23.15)$$

$$K_{mdk} = \frac{1}{2}K_1x_1^2 + \frac{1}{2}K_2x_2^2 + \frac{1}{2}K_{12}(x_1 - x_2)^2$$

where (m_b, k_b) are given by (23.7) and (m_{link}, k_{link}) are given by (23.14), respectively.

Comparing the energy expressions of the two models, it is clear that the degrees of freedom (x_3, x_4) which represent the transverse displacement at the junctions of the linking beam and the two resonator beams must be substituted by the mid-span displacements of the two beams, (x_1, x_2) . This can be accomplished by using the assumed displacement relation for the resonator beam given by (23.5):

$$x_3 = a x_1$$

$$x_4 = a x_2$$

$$a = N(\beta L, e)$$

$$N(\beta L, e) = \frac{\Phi(e)}{\Phi(L/2)}, \quad \beta L = 4.73$$

$$\Phi(L/2) = (\sin \beta L/2 - \sinh \beta L/2) + \frac{(\sin \beta L - \sinh \beta L)}{(\cos \beta L - \cosh \beta L)} (\cos \beta L/2 - \cosh \beta L/2)$$

$$\Phi(e) = (\sin \beta e - \sinh \beta e) + \frac{(\sin \beta L - \sinh \beta L)}{(\cos \beta L - \cosh \beta L)} (\cos \beta e - \cosh \beta e) \quad (23.16)$$

Table 23.1 Link offset amount (e) vs. Link factor (a)

| Link Offset (e) | Link Factor (a) | a^2 |
|-----------------|------------------|------------------|
| 0.0625 | 0.00906327886493 | 0.00008214302378 |
| 0.1250 | 0.03946457838609 | 0.00155745294719 |
| 0.1875 | 0.09611178177002 | 0.00923747459501 |
| 0.2500 | 0.18424759908145 | 0.03394717776728 |
| 0.3125 | 0.30988889279730 | 0.09603112587914 |
| 0.3750 | 0.48050748799022 | 0.23088744601468 |
| 0.4375 | 0.70599928850552 | 0.49843499537030 |
| 0.5000 | 1.00000000000000 | 1.00000000000000 |

The offset amount (e) vs. the link factor (a) for representative ranges are tabulated in Table 23.1 below.

Substituting ($x_3 = ax_1$, $x_4 = ax_2$) obtained in the above equation into the kinetic and potential energy expression of the skeletal model (23.14), we obtain

$$\begin{aligned}
 T_s &= \frac{1}{2}m_b\dot{x}_1^2 + \frac{1}{2}m_b\dot{x}_2^2 + \frac{1}{2} \begin{bmatrix} \dot{x}_1 \\ \dot{x}_2 \end{bmatrix}^T a^2 [m_{link}] \begin{bmatrix} \dot{x}_1 \\ \dot{x}_2 \end{bmatrix} \\
 K_s &= \frac{1}{2}k_b x_1^2 + \frac{1}{2}k_b x_2^2 + \frac{1}{2} \begin{bmatrix} x_1 \\ x_2 \end{bmatrix}^T a^2 [k_{link}] \begin{bmatrix} x_1 \\ x_2 \end{bmatrix}
 \end{aligned} \tag{23.17}$$

The above equation can be simplified by using (m_{link} , k_{link}) derived in (23.13) as

$$\begin{aligned}
 T_s &= \frac{1}{2}(m_b + a^2 m_s)\dot{x}_1^2 + \frac{1}{2}(m_b + a^2 m_s)\dot{x}_2^2 \\
 K_s &= \frac{1}{2}k_b x_1^2 + \frac{1}{2}k_b x_2^2 + \frac{1}{2}a^2 k_s (x_1 - x_2)^2
 \end{aligned} \tag{23.18}$$

Comparing (23.18) with the equivalent mass-damper-spring model (23.15), we find the following model parameters:

$$M_1 = M_2 = m_b + a^2 m_s = 0.3836 (\rho AL) + 0.24638 (a^2 \rho A_s L_s)$$

$$K_1 = K_2 = k_b = \frac{192EI}{L^3} \tag{23.19}$$

$$K_{12} = a^2 k_s = a^2 \left(\frac{12EI_s}{L_s^3} \right)$$

§23.5 A TWO-DOF MODEL AND EVALUATION OF RESONATOR PERFORMANCE

The quality of a resonator is quantified by the *Quality Factor*, Q , as defined by

$$\text{Q-Factor} = \frac{1}{2\zeta_{\text{system}}} \quad (23.20)$$

where ζ_{system} is the damping ratio with respect to the *center frequency* that is the average of the two peak resonances. It has been found that a major loss source is the energy transmission is from the resonator to the substrate, which is akin to the damping of machinery equipment to the ground due to vibrations discussed in Lecture 22.

The equations of motion for the two-DOF mass-damper-model shown in Fig. 22.11 can be derived as

$$\begin{bmatrix} M_1 & 0 \\ 0 & M_2 \end{bmatrix} \begin{bmatrix} \ddot{x}_1 \\ \ddot{x}_2 \end{bmatrix} + \begin{bmatrix} c_1 + c_{12} & -c_{12} \\ -c_{12} & c_2 + c_{12} \end{bmatrix} \begin{bmatrix} \dot{x}_1 \\ \dot{x}_2 \end{bmatrix} + \begin{bmatrix} K_1 + K_{12} & -K_{12} \\ -K_{12} & K_2 + K_{12} \end{bmatrix} \begin{bmatrix} x_1 \\ x_2 \end{bmatrix} = \begin{bmatrix} f_1 \\ 0 \end{bmatrix} \quad (23.21)$$

A word for the physical meaning of the two damping parameters: c_1 and c_2 act as if the damping is independent of each other, while c_{12} produces energy loss that is proportional to $(\dot{x}_1 - \dot{x}_2)$. Experiments of a series of double beam resonators indicate that the system loss is higher for the in-phase mode than the out-of-phase mode. Hence, we will drop c_{12} in subsequent analyses and set the two damping parameters to be the same

$$c_1 = c_2, \quad c_{12} = 0 \quad (23.22)$$

Table 23.2 Resonator Model Parameters

| L | b | $h = h_s$ | L_s | b_s | e | E | ρ |
|------------------|-----------------|-----------------|--------------------|-------------------|--------|---------|-----------------------|
| $40 \mu\text{m}$ | $8 \mu\text{m}$ | $2 \mu\text{m}$ | $11.8 \mu\text{m}$ | $2.7 \mu\text{m}$ | 0.25 L | 190 GPa | 2330 kg/m^3 |

Computations of the two degrees of freedom model using the model parameters listed in Table 23.2

give

$$\begin{aligned}
 m_b &= 5.720 \times 10^{-13}, & m_s &= 3.658 \times 10^{-14}, & k_s &= 2235 \text{ N/m} \\
 M_1 &= M_2 = 5.7451 \times 10^{-13} \text{ kg} \\
 K_1 &= K_2 = k_b = 2720.0 \text{ N/m} \\
 K_{12} &= a^2 k_s = 75.868 \text{ N/m}, & a^2 &= 0.03395 \text{ with } e = 0.25L \\
 \omega_{beam} &= \frac{1}{2\pi} \sqrt{k_b/m_b} = 10.975 \text{ (MHz)} \\
 \omega_{link} &= \frac{1}{2\pi} \sqrt{k_s/m_s} = 39.340 \text{ (MHz)}
 \end{aligned}
 \tag{23.23}$$

Note that the frequency of the linking beam is about three and half times larger than that of the two beam resonators, thus effectively avoiding mode coupling between them.

Figure 23.6 plots the transfer function (or FRF) of the output port, $(X_2(\omega)/(x_1)_{st})$, that is the ratio of the input signal with respect to the output signal ratio vs. the input signal frequency. For illustrative purposes, the damping $c_1 = c_2$ is parameterized by

$$\begin{aligned}
 c_1 = c_2 &= 2 \zeta m_b \sqrt{K_1/m_b} \\
 \zeta &= [0, 0.001, 0.005, 0.01, 0.05]
 \end{aligned}
 \tag{23.24}$$

Note that the model has two resonant peaks, (10.963, 11.264) MHz . Ideally the closer the frequency separation between the two peaks, the better the ability of the resonator to pick up the receiving frequency. A closer-up view of the two peak frequencies is shown in Fig. 23.7.

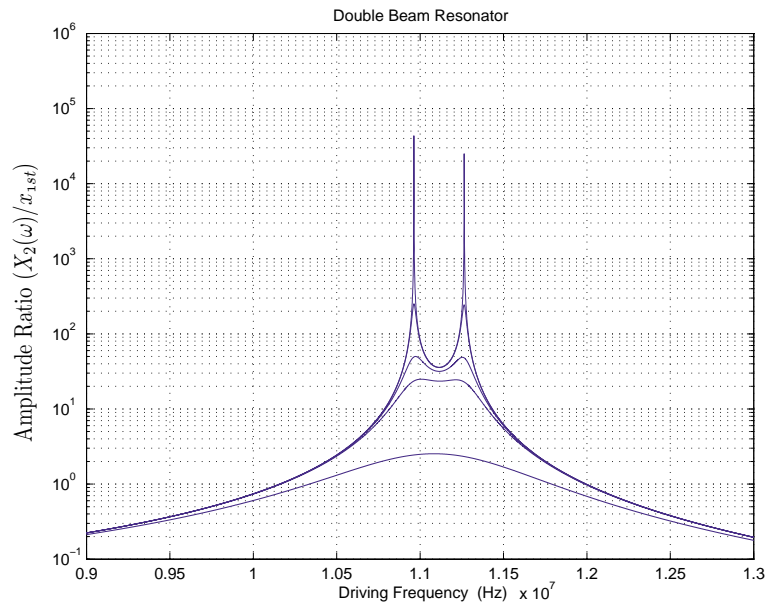


Figure 23.6: FRF from Input to the Output Signal, $H_{21}(\omega)$

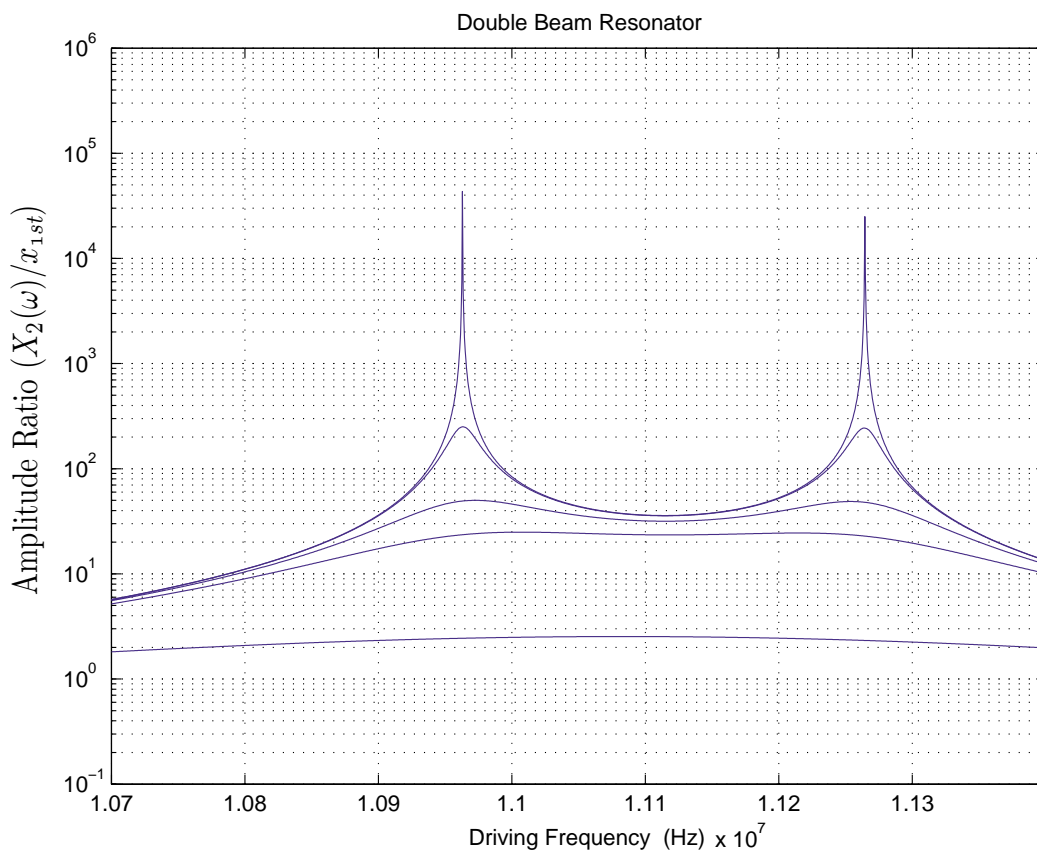


Figure 23.7: Closer-Up view of $H_{21}(\omega)$ Plot

In more realistic high-fidelity modeling, the lower-frequency peak is a little lower than that of the higher resonance. This is because the lower peak is associated with the in-phase mode and the higher with the out-of-phase mode, which causes less loss through the substrate. This is shown in an elaborate simulation that has been correlated with experimental data as shown in Fig.23.8. It should be noted that in the high-fidelity simulation, the electrostatic effects, the interaction with the substrate which absorbs the energy as it acts and flexible ground, etc. have been modeled in an elaborate way.

The high-fidelity model and its performance assessment is shown in Fig.23.9.

In conclusion, a simple two-DOF model can be used to size up the design, peak frequencies, and the position to how to anchor the beams, and the amount of energy loss. It turns out that resonators can also be designed by exploiting the den Hartog invariant points, this time by maximizing its two peaks rather than by minimizing its peak. This is beyond the scope of this course and left as research topics to those interested in the resonator design.

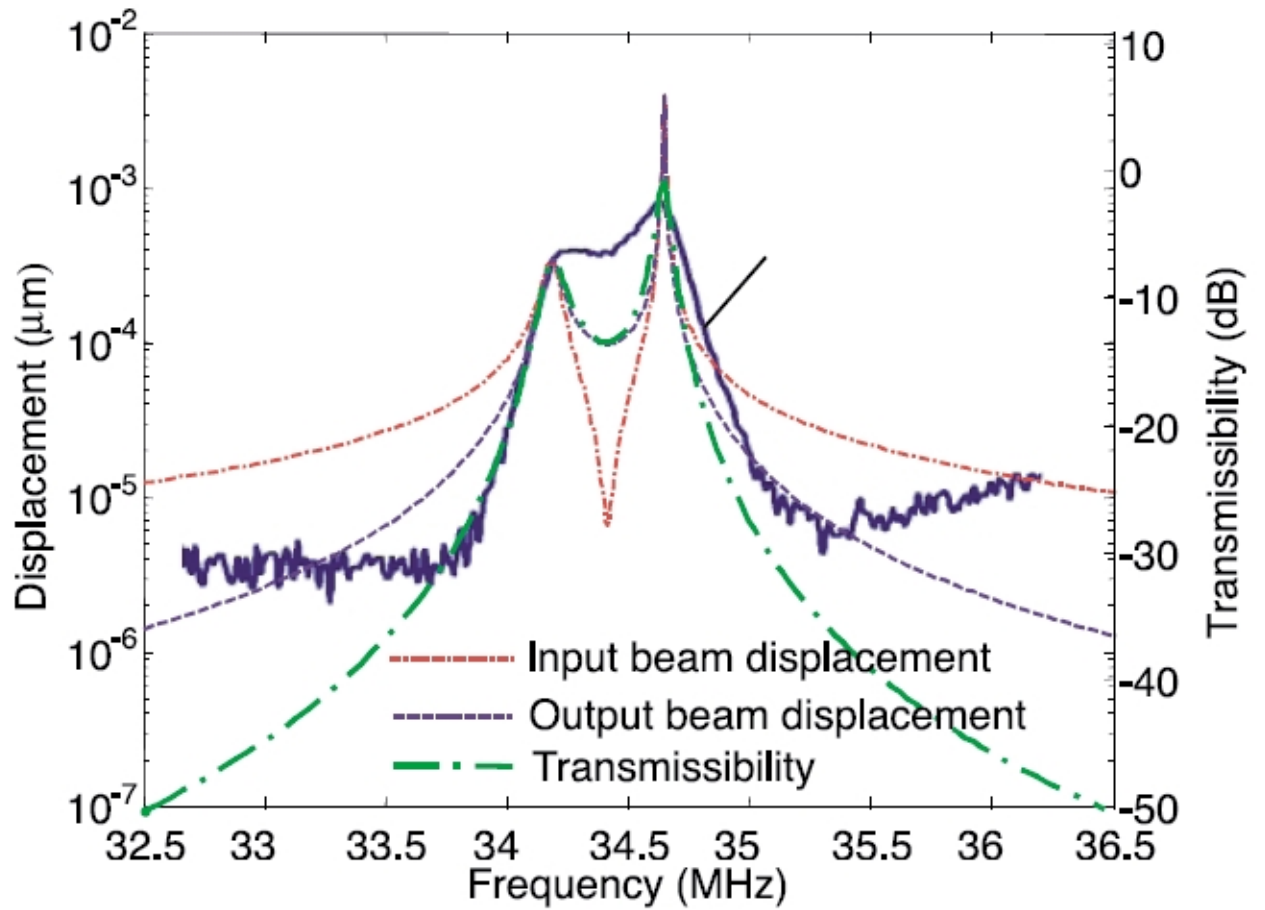


Fig. 11. Displacements at the input-output beam electrodes and the transmissibility of experiment and that of the simulation with the substrate effect (flexible substrate).

Figure 23.8: High-fidelity model of a resonator and its correlation with experimental data

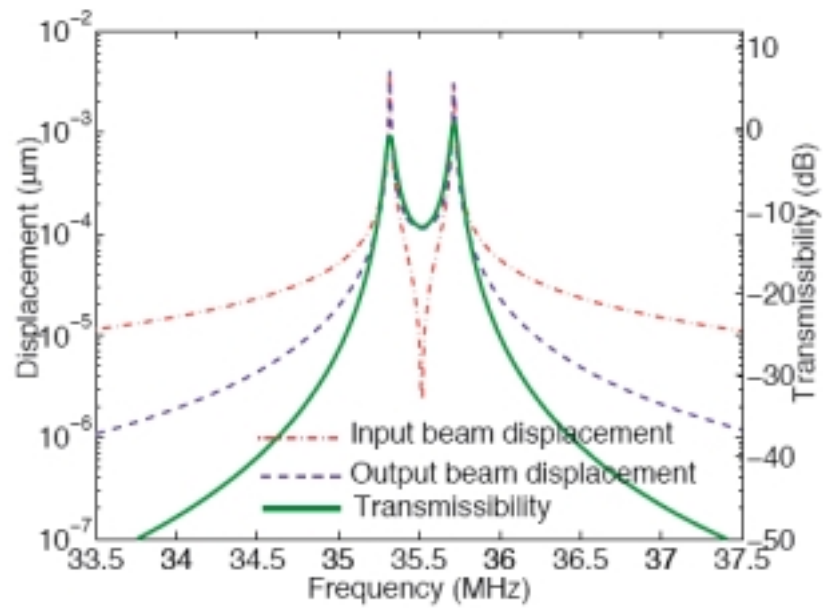


Fig. 12. Displacements at the input-output beam electrodes and the transmissibility of the simulation without the substrate effect (rigid substrate).

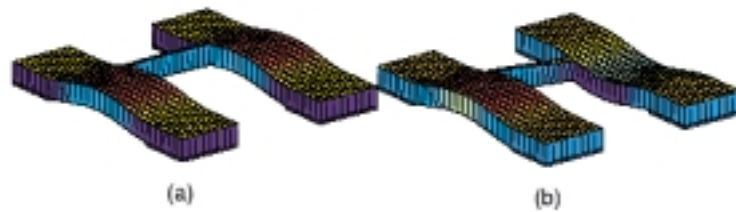


Fig. 13. Layout of the finite element model and the deformations of the paired-beam resonator at two resonant modes. (a) First mode: in-phase beam motion ($f_1=34.18\text{MHz}$); (b) second mode: out-of-phase beam motion ($f_2=34.65\text{MHz}$).

Figure 23.9: A refined model and the performance curves